Analysis of in-situ combustion of oil with pyrolysis and vaporization*

A.A. Mailybaev†, J. Bruining‡, D. Marchesin§

May 3, 2011

Abstract

We study one-dimensional flows, when air is injected into a porous medium filled with inert gas, medium or high viscosity oil and water, giving rise to a combustion wave in a process known as high-temperature oxidation (HTO). In the oil we distinguish three pseudo-components: asphaltenes, medium and light oil. At high temperatures, the heaviest components ("precoke") are converted to coke, which undergoes combustion. Medium oil components are cracked at intermediate temperatures releasing gaseous oil. Light oil components and water are vaporized. The oxidation rate of gaseous oil components is negligible. Combustion regimes are described in the form of a sequence of waves. We develop a simple mathematical pathway based on Zeldovich's approach to provide analytical formulae for parameters in these waves. It is shown that there is a combustion regime in which either coke or oxygen are partially consumed in the combustion as well as a regime in which both are consumed completely. Each of the regimes can be subdivided in two regimes, where the reaction is either trailing or leading with respect to the thermal wave. Explicit conditions for each combustion regime are given. The structure of the oil cracking layer is investigated. Stability of the solutions is studied. We analyse our formulae for typical in-situ combustion data and compare the results with numerical simulations.

keyword in-situ combustion; porous medium; filtration; traveling wave; combustion regimes; stability; heavy oil; cracking; vaporization

Nomenclature

t	time (s)
x	spatial coordinate (m)
c_g	heat capacity of gas (J/mol K)
C_m	heat capacity of porous medium (J/m^{3}K)
E_c	cracking activation energy (J/mol)
E_h	HTO activation energy (J/mol)
K_c	cracking pre-exponential factor (1/s)
K_h	HTO pre-exponential factor (1/s)
M_c	average molar weight of cracked oil (kg/mol)
M_h	molar weight of carbon (kg/mol)
M_v	average molar weight of light oil/water (kg/mol)
n_h	precoke (carbon) concentration (kg/m^3)
n_c	medium oil concentration (kg/m^3)
n_v	light oil concentration (kg/m^3)
P_{tot}	prevailing pressure of gas (Pa)
Q_h	HTO reaction enthalpy (J/kg)
Q_c	cracking reaction enthalpy (J/kg)
Q_v	vaporization heat (J/kg),
R	ideal gas constant (J/mol K)
T	temperature (K)
T_{st}	reference temperature (K)
u	gas Darcy velocity (m/s)
Y	molar fraction of oxygen in gas (mol/mol)
λ	thermal conductivity of porous medium (W/mK)
ρ	molar density of gas (mol/m^3)
φ	porosity
W_h	HTO rate (kg/m$^3 s$)
W_c	cracking rate (kg/m$^3 s$)
W_v	vaporization rate (kg/m$^3 s$)
inj	injection conditions (subscript)
unb	unburned part of a reactant (sub- or superscript)

*This work was supported in part by: CNPq under Grants 474121/2008-9, 314583/2009-2, 301564/2009-4, FAPERJ under Grants E-26/110.310/2007, E-26/110.972/2008, E-26/102.723/2008, E-26/112.220/2008, E-26/112.112/2008, and the President of Russian Federation grant MK-4244.2008.1. The authors also thank IMPA and TUDelft for hospitality during the visits.

†Institute of Mechanics, Moscow State University, Michurinsky pr. 1, 119192 Moscow, Russia. E-mail: mailybaev@imec.msu.ru

‡TU Delft, Civil Engineering and Geosciences, Stevinweg 1, 2628 CE Delft, The Netherlands. E-mail: J.Bruining@tudelft.nl

§Instituto Nacional de Matematica Pura e Aplicada, Estrada Dona Castorina 110, 22460-320 Rio de Janeiro, RJ, Brazil. E-mail: marchesi@impa.br

Dimensionless variables

θ	temperature
θ_v	vapor zone temperature
m	gas flux

1 Introduction

There is renewed interest in developing methods to recover "difficult oil". One of the options to recover medium viscosity oil, i.e., oil with a viscosity lower than 10^4 [cP], is the application of air injection [1, 2, 3, 4, 5, 6, 7]. It is proposed that the oxygen in the air burns the heavier components of oil, generating a heat wave leading to cracking and vaporization of lighter components. Studying a one dimensional version of this flow would reveal some mechanisms in the combustion process. Even in 1-D this is not a trivial problem, because combustion, cracking, etc., occur in regions with narrow width, leading to a tough multi-scale problem [8, 9, 10, 11, 12]. For this reason it is useful to develop analytical models that can be used to validate numerical results and for assessing the risk of oxygen breakthrough [13, 14], a serious hazard in the application of this technique.

Analytical studies of steady combustion waves in a porous medium containing solid fuel were performed for forward [15] and counterflow [16] combustion, as well as for buoyant combustion [17, 18]. Transition to flaming was analyed in [19]. Intermediate resonant regimes leading to maximal energy accumulation were investigated in [20]. Periodic and other non-steady combustion regimes were investigated in [21, 22].

Note that in petroleum field applications of in-situ combustion heat losses are very small. However, they may become significant in laboratory experiments. The effect of heat losses for coke combustion was studied in [23]. Heat losses also prevent unlimited increase of temperature in the resonance regime [20].

A wave structure analysis within a narrow combustion layer is necessary representing the major mathematical difficulty. The typical approach uses a sheet approximation for the reaction region, e.g., [24], or large activation energy asymptotic expansion, e.g., [15]. Reaction-leading or reaction-trailing wave structures are usually identified, which correspond to partial oxygen or partial fuel consumption in the reaction for our problem. Additional physical processes may influence the combustion, e.g., multiple reactions [25, 26, 27, 28, 29], effects of solid conversion [30], gas–solid nonequilibrium [24], and vaporization of liquid (water) initially present in the reservoir [31] or injected with air [32, 33]. Similar analyses have been applied in problems of polymerization [34, 35] and smoldering of polyurethane foam, e.g., [36].

We analyse a three pseudo-component model for crude oil in-situ combustion presented in [14]. The pseudo-components are distinguished according to the types of reaction in which they participate, viz., HTO, cracking and vaporization. The gas phase contains oxygen, gaseous oil, steam, combustion products (carbon dioxide) and inert gas, e.g., N_2. In some combustion regimes, oxygen may be present in the gas together with gaseous light oil, potentially leading to oxidation. However, the oxidation in the gaseous phase can be ignored in in-situ combustion applications; this reaction is suppressed because of small pore size. Such a model allows describing the internal structure of the combustion wave relative to HTO, cracking and vaporization, which is our contribution.

We approximate the solution of the combustion process as a sequence of thermal and combustion waves traveling with constant speeds and separated by a constant state (hot) region in between. In this paper we take the reservoir state ahead of the sequence of waves as given. Otherwise, one would require an extension of the present model to include flow, condensation and slow oxidation reactions in the reservoir at relatively low temperatures, which is a separate problem. Based on the large activation energy asymptotic approach, we develop a simplified method for the analysis of combustion waves. It allows a simple mathematical pathway providing a series of analytical expressions for in-situ combustion.

Using this method, we derive explicit formulae for the dependent variables in the waves and classify possible combustion regimes. As in previous studies (e.g., [15, 24, 32]), we distinguish the reaction-leading and reaction-trailing structures. For both structures, our method allows to identify a relatively wide range of parameters, corresponding to essentially complete consumption of both oxygen and coke in the HTO reaction. We also describe in detail the structure of the cracking region, and estimate the effect of oil vaporization. Stability of the resulting solutions is studied analytically.

The structure of the paper is as follows. Section 2 describes the model and the reduction of its equations to a dimensionless form. In Section 3, we study combustion solutions with a reaction-leading wave sequence, i.e., where the HTO reaction occurs at the upstream part of the sequence. Section 4 studies solutions with a reaction-trailing wave sequence. In Section 5 we give stability conditions for the solutions obtained. Section

6 presents the results of numerical calculations with typical reservoir data for in-situ combustion. We end with some conclusions. The Appendices provide the study of the cracking layer in more detail and the stability analysis of steady combustion waves.

2 Model

Models of in-situ combustion in oil reservoirs have several properties distinguishing them from smoldering problems in other environments like polyurethane foams, SHS, etc.. The usual set of assumptions includes (see, e.g., [23]): large volumetric rock heat capacity, limited fuel availability in certain cases, small pore sizes suppressing reactions in the gas phase, small heat radiation effects in the rock, large prevailing pressures with small relative variations, small changes of porosity and permeability in the combustion process, and small heat losses.

The subject of our study are flows possessing a combustion wave when a gaseous oxidizer (air) is injected into the porous medium, a rock cylinder thermally insulated preventing lateral heat losses and filled with gas, some crude (medium viscosity) oil, and water. The case of forward combustion when the ignition occurs at the injection side is considered. In our study of combustion, the mobility of any components other than gas will be ignored, because it is assumed that the speed of the reaction wave exceeds substantially the speed of any liquids.

Oil consists of multiple components: asphaltenes, volatiles, saturates, aromatics, resins, etc.. We will consider a reaction scheme comprising high-temperature oxidation (HTO), cracking and vaporization. The oil components will be grouped accordingly into three pseudo-components called precoke, medium and light oil.

Precoke includes the heaviest (asphaltene) components, which are converted to coke at high temperatures, releasing gaseous hydrocarbons. The gaseous mass and heat exchanges in this process are small and can be neglected, so we include coke into the same precoke pseudo-component. We describe precoke in terms of the corresponding carbon concentration n_h. The combustion of coke in the presence of oxygen (HTO) gives rise to the highest temperatures present in the combustion process. We model HTO as a single reaction

$$C + O_2 \to CO_2. \tag{2.1}$$

The lighter components, which are vaporized ahead of the combustion layer, are grouped into the light oil pseudo-component with concentration n_v. If water is present, we include it into the n_v component. The remaining parts form a medium oil pseudo-component with concentration n_c. As temperature increases, the medium oil cracks into lighter components, which are released as vapor. The concentrations n_h, n_c, n_v are expressed in terms of [kg/m^3 of porous medium].

Transport of oil by convection is disregarded, as explained above. Therefore, it is possible to write the rate of change of the oil concentrations in terms of the reaction rates W [kg/m^{3}s] as follows

$$\frac{\partial n_h}{\partial t} = -W_h, \quad \frac{\partial n_c}{\partial t} = -W_c, \quad \frac{\partial n_v}{\partial t} = -W_v. \tag{2.2}$$

As to the gas composition, we distinguish between the molar fraction Y of oxygen and the remaining non-reactive gas fraction $1 - Y$ that consists of vaporized oil, steam, combustion products and initial inert gas. The mass balance equations for the gas fractions are

$$\varphi \frac{\partial}{\partial t}(1-Y)\rho + \frac{\partial}{\partial x}(1-Y)\rho u = \frac{W_h}{M_h} + \frac{W_c}{M_c} + \frac{W_v}{M_v}, \tag{2.3}$$

$$\varphi \frac{\partial}{\partial t} Y\rho + \frac{\partial}{\partial x} Y\rho u = -\frac{W_h}{M_h}, \tag{2.4}$$

with the constant rock porosity φ and gas density $\rho = P_{tot}/RT$. Pressure variations are assumed to be small, so we take $P_{tot} = const$. We ignored diffusion in (2.3), (2.4). For the most typical reaction-leading wave structure, diffusion effects are unimportant as will be justified later. For the reaction-trailing wave structure, the case when diffusion is dominant in the HTO layer requires a separate study. The sum of (2.3) and (2.4) gives the mass balance for the total gas

$$\varphi \frac{\partial \rho}{\partial t} + \frac{\partial \rho u}{\partial x} = \frac{W_c}{M_c} + \frac{W_v}{M_v}. \tag{2.5}$$

Here the W_h term cancels out as the HTO reaction (2.1) produces no net gas in moles.

Assuming that the temperature of solid rock, liquid oil/water and gas are equal and neglecting heat losses, we write the heat transport equation as

$$C_m \frac{\partial T}{\partial t} + c_g \frac{\partial}{\partial x} \rho u (T - T_{st}) = \lambda \frac{\partial^2 T}{\partial x^2} + Q_h W_h - Q_c W_c - Q_v W_v. \tag{2.6}$$

The heats Q_h, Q_v are positive; in most situations Q_c is also positive. In the accumulation term, we ignore gas, water and oil heat capacities compared to rock heat capacity. Therefore, the heat capacity per unit volume of the porous medium is taken approximately equal to the constant heat capacity of the rock C_m. The gas heat capacity is taken approximately as $c_g \approx 3.5R$, ignoring small variations of heat capacity among different gas components. The fact that heat capacities are constant is used to write (2.6) in a simple form.

Note that the form of the left-hand side of (2.6) corresponds to constant reaction heats (enthalpies) Q_h, Q_c, Q_v taken at standard conditions for the temperature T_{st}. If these reaction heats are evaluated at the actual temperature T, the left-hand side becomes $C_m \partial T/\partial t + c_g \rho u \partial T/\partial x$, as one can show using the mass balance equations (2.2)–(2.5).

Arrhenius' law and the assumption of a linear dependence on the fuel concentration and oxygen concentration lead to

$$W_h = K_h Y n_h \exp\left(-\frac{E_h}{RT}\right). \tag{2.7}$$

For the cracking reaction rate, one can assume

$$W_c = K_c n_c \exp\left(-\frac{E_c}{RT}\right). \tag{2.8}$$

We will not need an expression for vaporization rate, because it affects only the internal structure of the condensation wave, which is not relevant here.

The variables to be found are the temperature T, the concentrations n_h, n_c, n_v, Y and the Darcy velocity u. All the coefficients in the equations (C_m, c_g, λ, etc.) are assumed to be constant. The air injection is characterized by the Darcy velocity u_{inj}, oxygen fraction Y_{inj} and temperature T_{inj}.

2.1 Dimensionless equations

The governing equations are non-dimensionalized by introducing dimensionless dependent and independent variables as ratios of dimensional quantities and reference quantities:

$$\begin{gathered} \tilde{t} = \frac{t}{t^*},\ \tilde{x} = \frac{x}{x^*},\ \theta = \frac{T - T_{st}}{T^*},\ m = \frac{\rho u}{m^*}, \\ \tilde{n}_h = \frac{n_h}{n_h^*},\ \tilde{n}_c = \frac{n_c}{n_c^*},\ \tilde{n}_v = \frac{n_v}{n_v^*}, \end{gathered} \tag{2.9}$$

where $m^* = u_{inj} P_{tot}/RT_{st}$ is the injected gas flux. We take $v^* = c_g m^*/C_m$, which turns out to be the speed of the thermal wave in a reservoir with no oil. Then we introduce the reference length $x^* = \lambda/(C_m v^*)$, which is related to the length of the conduction zone of the combustion wave, and the corresponding reference time $t^* = x^*/v^*$. We choose $T^* = Q_h n_h^*/C_m$ which is the temperature change for combustion under adiabatic conditions. As the model presented here does not include the condensation zone, the reference concentrations n_h^*, n_c^*, n_v^* will be specified later as input concentrations far downstream of the combustion wave.

In the left-hand side of (2.3)–(2.5), the accumulation terms are negligible relative to the flux terms because the relation between the gas speed u and wave speed $v = dx/dt$ turns out to be $v/u \sim 10^{-3}$ in our applications. Therefore, we neglect these small terms from now on. Using (2.9) and omitting the tildes in

the dimensionless quantities, equations (2.4)–(2.6) and (2.2) are written in dimensionless form as

$$\frac{\partial \theta}{\partial t} + \frac{\partial m\theta}{\partial x} = \frac{\partial^2 \theta}{\partial x^2} + w_h - q_c w_c - q_v w_v, \tag{2.10}$$

$$\frac{\partial m}{\partial x} = \gamma_c w_c + \gamma_v w_v, \tag{2.11}$$

$$\frac{\partial Y m}{\partial x} = -\gamma_h w_h, \tag{2.12}$$

$$\frac{\partial n_h}{\partial t} = -w_h, \tag{2.13}$$

$$\frac{\partial n_c}{\partial t} = -w_c, \tag{2.14}$$

$$\frac{\partial n_v}{\partial t} = -w_v \tag{2.15}$$

with dimensionless parameters

$$\begin{gathered} q_c = \frac{Q_c n_c^*}{C_m T^*},\ q_v = \frac{Q_v n_v^*}{C_m T^*},\ \theta_0 = \frac{T_{st}}{T^*},\ \theta_{inj} = \frac{T_{inj}}{T^*}, \\ \gamma_h = \frac{c_g n_h^*}{C_m M_h},\ \gamma_c = \frac{c_g n_c^*}{C_m M_c},\ \gamma_v = \frac{c_g n_v^*}{C_m M_v}, \\ N_h = t^* K_h,\ N_c = t^* K_c,\ \mathcal{E}_h = \frac{E_h}{RT^*},\ \mathcal{E}_c = \frac{E_c}{RT^*}. \end{gathered} \tag{2.16}$$

Here q_c (q_v) are the ratios between the heat of cracking (vaporization) and the heat of combustion. The quantities $\gamma_h, \gamma_c, \gamma_v$ characterize reduced fluxes with which the precoke, the intermediates and the volatiles enter the moving combustion structure. They are normalized with respect to the air injection flux. For this interpretation we use $c_g/C_m = v^*/m^*$, where m^* is the air injection flux. The quantities N_h and N_c are related to Damköhler numbers, the ratios between reaction rates and the convective transport rate. The quantities $\mathcal{E}_h$ and $\mathcal{E}_c$ relate the activation temperatures E_h/R and E_c/R to the temperature increase due to the reaction. The dimensionless reaction rates are $w_h = t^* W_h/n_h^*$, $w_c = t^* W_c/n_c^*$, and $w_v = t^* W_v/n_v^*$ with

$$w_h = N_h Y n_h \exp\left(-\frac{\mathcal{E}_h}{\theta + \theta_0}\right), \tag{2.17}$$

$$w_c = N_c n_c \exp\left(-\frac{\mathcal{E}_c}{\theta + \theta_0}\right). \tag{2.18}$$

The boundary condition expressing air injection is described as

$$x = 0: \quad \theta = \theta_{inj}, \quad m = 1, \quad Y = Y_{inj}. \tag{2.19}$$

The initial reservoir is characterised by uniform distributions of temperature θ and oil concentrations n_h, n_c, n_v, except for the fact that at $t = 0$ there must be a small region of ignition near the injection point that allows for the formation of the combustion wave. We will study the solution as a sequence of separate waves that develop at large times.

3 Reaction-leading structure

Solution with reaction-leading structure is shown schematically in Fig. 1. Here the (slowest) thermal wave is determined by heat convection only. Along this wave the temperature decreases from a high combustion temperature θ_h to an injected gas temperature θ_{inj}. All oil has been removed from the region where this wave moves, so that the reaction rates are zero $w_h = w_c = w_v = 0$ and the mass flux remains constant, $m = 1$. Then (2.10) has solution $\theta(t, x) = \frac{1}{2}(\theta_h + \theta_{inj}) + \frac{1}{2}(\theta_h - \theta_{inj})\,\mathrm{erf}((x - t)/2\sqrt{t})$ describing a thermal wave moving with dimensionless speed $v_T = 1$.

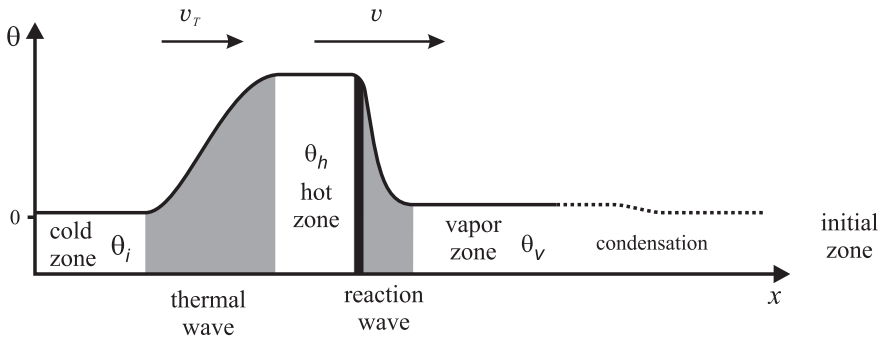

Figure 1: Temperature vs. distance for the reaction-leading structure. The reaction wave is faster than the thermal wave; the narrow layer in the reaction wave, where the HTO reaction occurs, is shown by the black bar. The cold and hot zones contain injected air. The vapor zone contains oleic, aqueous and gaseous phases. The latter contains oil vapor, steam and combustion products. The internal structure of the reaction wave is described in Fig. 2.

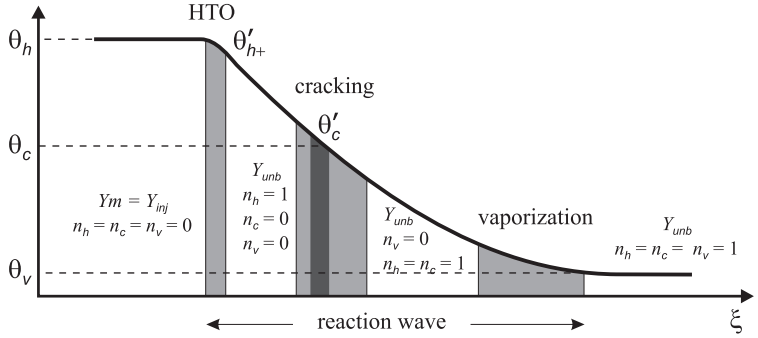

Figure 2: Blow-up of Fig. 1 with $\xi = x - vt$. Reaction wave internal structure: HTO, cracking and vaporization layers (indicated in grey). The HTO reaction occurs in a narrow layer at the highest temperatures. Cracking of each component occurs at a certain temperature θ_c within the cracking layer. The values of the oxygen flux Ym and the oil components concentrations n_h, n_c, n_v are specified in each region.

Ahead of the intermediate hot zone there is a reaction wave with speed $v > 1$. This wave occurs in wide range of temperatures and encompasses the HTO reaction, oil cracking and vaporization. The HTO reaction takes place in a thin layer corresponding to a small interval of the highest temperatures. The HTO layer is preceded by layers where cracking and vaporization occur, see Fig. 2. The presence of a hot zone containing oxygen behind the reaction wave ensures that all coke is consumed in the HTO reaction. Oxygen consumption is not necessarily complete, so the HTO reaction is coke limited.

Ahead of the reaction wave the temperature drops to the vapor zone value θ_v. The vapor zone contains oil and water in both liquid and gaseous forms. In the presence of oxygen (that may partially pass through the reaction wave), slow oxidation occurs in the vapor zone at lower temperatures. When the gas reaches the original cold reservoir, part of the oil vapor condenses. The oil concentrations in the vapor zone as well as the temperature θ_v are determined by the condensation and flow processes far ahead of the reaction wave, which represent a separate problem. In our study of combustion, we assume these quantities to be given.

Such a solution structure is called reaction-leading because combustion occurs ahead of the hot zone. As we will see below, the reaction-leading structure occurs when

$$Y_{inj} > \gamma_h. \tag{3.1}$$

This condition was also derived, e.g., in [15, 37, 38, 39] for similar problems. Note that (3.1) is satisfied in most practical situations, unless the injected gas contains very little oxygen. Physically, γ_h/Y_{inj} is the "flux" of coke with respect to the moving thermal wave divided by the oxygen flux. If this ratio is smaller than one, we need a higher coke "flux" and hence the reaction wave moves ahead of the thermal wave.

The unknown parameters of the reaction wave to be determined are the temperature θ_h, the wave speed v, the flux change in the wave and Y_{unb}, the amount of oxygen that passes unburned through the reaction wave.

We assume that the reaction wave has a traveling wave form, i.e., all quantities depend on a single traveling variable $\xi = x - vt$. In the hot zone behind the reaction wave, the porous medium contains only injected air: $m = 1$, $Y = Y_{inj}$, $n_h = n_c = n_v = 0$. In the vapor zone ahead of the wave, there are liquid oil, liquid water and gas. The gas contains combustion products, light oil vapor, steam, and possibly some oxygen. We take the concentrations of the oil pseudo-components in the vapor zone as the reference quantities n_h^*, n_c^*, n_v^* in (2.9). Thus, in the vapor zone, the dimensionless concentrations are $n_h = n_c = n_v = 1$.

3.1 High-temperature oxidation layer

The layer where HTO takes place contains coke, injected gas with oxygen, combustion products and some inert gas. As all medium and light oil components have been cracked and vaporized ahead of the HTO layer, $n_c = n_v = 0$, hence, $w_c = w_v = 0$. The molar gas flux m is equal to one, as follows from (2.11). It remains constant because one mole of O_2 is converted to one mole of CO_2. The coke concentration in the layer changes from $n_h = 1$ to 0 and the oxygen fraction in the gas changes from the mole fraction left unburned after passing the HTO layer to the injected mole fraction, i.e. from Y_{unb} to Y_{inj}.

The reaction rate w_h in (2.17) has a strong temperature dependence determined by the argument of the exponential factor. Therefore we can only afford a very small temperature variation $\delta\theta_h$ in the HTO layer, before the reaction rate becomes negligible. Expanding the exponent near the temperature of the hot zone θ_h, for small $\delta\theta = \theta_h - \theta$ we find

$$\exp\left(\frac{-\mathcal{E}_h}{\theta + \theta_0}\right) \approx \exp\left(\frac{-\mathcal{E}_h}{\theta_h + \theta_0}\right) \exp\left(\frac{-Z_h \delta\theta}{\theta_h - \theta_v}\right), \tag{3.2}$$

$$Z_h = \frac{\mathcal{E}_h(\theta_h - \theta_v)}{(\theta_h + \theta_0)^2}, \tag{3.3}$$

where $Z_h \gg 1$, because the activation energy $\mathcal{E}_h$ is large (a typical value is $Z_h \approx 15$). The exponential containing Z_h is a reduction factor in the reaction rate. When the reduction factor becomes small enough the reaction no longer contributes. Arbitrarily we choose this threshold at $\exp(-1)$. Thus, the reaction occurs within a small temperature interval $\delta\theta_h \sim (\theta_h - \theta_v)/Z_h$ corresponding to a change of order 1 in the exponent; the reaction rate decreases exponentially and can be neglected for $\theta_h - \theta \gg \delta\theta_h$. The quantity Z_h is the Zeldovich number, the ratio between the total temperature variation in the wave and the temperature variation in the HTO layer [9]. Using the expression for $\delta\theta_h$, we find that the HTO reaction is confined within the space interval

$$\delta\xi_h \sim \frac{\delta\theta_h}{|\theta_h'|} \sim \frac{\theta_h - \theta_v}{Z_h|\theta_h'|}, \tag{3.4}$$

where $|\theta_h'|$ is the effective temperature gradient in the HTO layer. For $Z_h \gg 1$, $\delta\xi_h$ is much smaller than the width of the whole wave, estimated as $(\theta_h - \theta_v)/|\theta_h'|$. Thus, the HTO layer is narrow indeed.

Substituting w_h from (2.17) into (2.12) with $m = 1$ and using the traveling wave coordinate $\xi = x - vt$, we obtain

$$\frac{\partial \log Y}{\partial x} = \frac{d \log Y}{d\xi} = -\gamma_h N_h n_h \exp\left(-\frac{\mathcal{E}_h}{\theta + \theta_0}\right). \tag{3.5}$$

Since n_h changes from 1 to 0, its average value is $n_h \sim 1/2$. Taking

$$\frac{d \log Y}{d\xi} \sim \frac{\log Y_{inj} - \log Y_{unb}}{\delta\xi_h} = \frac{1}{\delta\xi_h} \log\left(\frac{Y_{inj}}{Y_{unb}}\right)$$

and $\theta \approx \theta_h$ in (3.5) with Z_h and $\delta\xi_h$ and from (3.3), (3.4) gives

$$\log \frac{Y_{inj}}{Y_{unb}} \sim \frac{\gamma_h A_h}{Y_{inj}}, \tag{3.6}$$

$$A_h = \frac{(\theta_h + \theta_0)^2 N_h Y_{inj}}{2\mathcal{E}_h|\theta_h'|} \exp\left(-\frac{\mathcal{E}_h}{\theta_h + \theta_0}\right). \tag{3.7}$$

Using the estimate in (3.6), we can distinguish two regimes according to the values of ratio Y_{unb}/Y_{inj} between the oxygen fraction remaining downstream of the HTO layer (unburned oxygen) and the oxygen fraction in the injected air. The importance of this ratio has been recognized in different contexts, e.g., [24, 26, 28, 36].

The first regime is characterized by almost complete consumption of oxygen in the HTO layer, $Y_{unb} \ll Y_{inj}$, and corresponds to high combustion temperatures θ_h (and according to Eq. (3.6) to large A_h). The condition for this regime follows from (3.6); it is approximately

$$\frac{\gamma_h A_h}{Y_{inj}} > 1. \tag{3.8}$$

Due to the strong exponential dependence of A_h on the combustion temperature θ_h in (3.2), one can show that this approximation distinguishes the two regimes with an uncertainty of order Z_h^{-1}. This number is also the width of the narrow transition zone between the regimes. Since almost all the oxygen is consumed, the reaction ahead of the HTO layer stops primarily due to lack of oxygen. Hence, the HTO layer width is smaller than $\delta\xi_h$ obtained in (3.4) based on the temperature dependence of the reaction rate. Note that, in this regime, coke is consumed completely too, giving rise to an "optimal" combustion regime with consumption of both reactive components. Such regimes are called stoichiometric or filtration-controlled, see, e.g., [15, 24]. As we will see later, the complete coke and oxygen consumption regime occurs for a relatively wide range of problem parameters separating the cases of oxygen limited and coke limited combustion.

In the second regime (3.8) is not satisfied. In this case, the HTO reaction stops due to low temperatures when both coke and oxygen are still present (kinetically-controlled regime, see, e.g., [15, 24]). Since a substantial part of the oxygen is not consumed in the HTO, we can use $Y \sim Y_{inj}$ and $n_h \sim 1/2$ estimating the reaction rate in (2.17) as

$$w_h \sim N_h(Y_{inj}/2)\exp(-\mathcal{E}_h/(\theta_h + \theta_0)).$$

Then equation (2.13) with $\partial n_h/\partial t \sim 1/\delta t_h \sim v/\delta\xi_h$ and (3.4), (3.3) yield the relation $v \sim A_h$ with A_h given by (3.7). Using (3.2), one can show that pretending that v and A_h are actually equal leads to an error of order Z_h^{-1} in the temperature value θ_h. This justifies writing this relation approximately as

$$v = A_h. \tag{3.9}$$

Note that (3.9) can also be obtained by solving the differential equations for the traveling wave in the HTO layer as in [15, 24, 31].

The unburned oxygen fraction Y_{unb} can be found from the mass balance. Equation (2.12) with w_h expressed from (2.13) yields $(Ym)' = -\gamma_h v n_h'$, where the prime denotes the derivative with respect to the traveling coordinate $\xi = x - vt$, and we used $\partial/\partial x = d/d\xi$, $\partial/\partial t = -vd/d\xi$. Integrating this equation across the HTO layer, where Y changes from Y_{inj} to Y_{unb}, n_h changes from 0 to 1, and $m = 1$ remains unchanged (see Fig. 2), we obtain

$$Y_{unb} = Y_{inj} - \gamma_h v. \tag{3.10}$$

Using the conditions $v > 1$ and $Y_{unb} > 0$ in (3.10), we confirm the inequality (3.1). Note that (3.10) with v from (3.9) yields $Y_{unb} = 0$ at the threshold given by (3.8) written as an equality.

Similarly, using rates expressed from (2.13)–(2.15) and $\partial/\partial x = d/d\xi$, $\partial/\partial t = -vd/d\xi$ in (2.10), we obtain

$$\big(\theta' + (v - m)\theta) + v(n_h - q_c n_c - q_v n_v)\big)' = 0. \tag{3.11}$$

Integration of (3.11) across the HTO layer, where n_h changes from 0 to 1, θ' changes from 0 to θ'_{h+}, while $m = 1$ and $n_c = n_v = 0$ remain unchanged (see Fig. 2), yields

$$\theta'_{h+} = -v, \tag{3.12}$$

ignoring a small temperature variation $\delta\theta_h$. Since the temperature gradient in the HTO layer changes from (3.12) to $\theta' = 0$, its average value to be used in (3.7) is

$$|\theta'_h| = v/2. \tag{3.13}$$

Finally, let us consider the effect of oxygen diffusion, which was neglected in equation (2.4). One can show that diffusion has no influence on the description of the HTO layer we presented, within the accuracy of the method. Indeed, in the case of partial oxygen consumption, when $Y_{unb} \sim Y_{inj}$, the variation of Y due to diffusion is not important for the result (3.9), which was obtained using order-of-magnitude estimates and exploiting the strong exponential dependence of combustion rate on temperature. Using (3.9) in (3.10), we obtain $Y_{unb} > 0$ only if $\gamma_h A_h/Y_{inj} < 1$. Therefore, the condition (3.8) for complete oxygen consumption remains valid when gas diffusion is taken into account.

3.2 Reaction wave for complete coke/oxygen consumption

Let us consider the case (3.8), when all oxygen is consumed in the HTO layer. The wave speed is found by taking $Y_{unb} = 0$ in (3.10) as

$$v = Y_{inj}/\gamma_h. \tag{3.14}$$

Integrating (3.11) across the whole reaction wave yields

$$[\theta'] + v[\theta] - [m\theta] + v([n_h] - q_c[n_c] - q_v[n_v]) = 0, \tag{3.15}$$

where the square brackets denote the variation of the quantity in the wave. Using in (3.15) the conditions $[\theta'] = 0$, $[\theta] = \theta_v - \theta_h$, $[m\theta] = m_v\theta_v - \theta_h$, and $[n_h] = [n_c] = [n_v] = 1$, where m_v denotes the gas flux ahead of the wave, we obtain

$$\theta_h = \frac{v(q + \theta_v) - \theta_v m_v}{v - 1} \quad \text{with} \quad q = 1 - q_c - q_v. \tag{3.16}$$

The quantity q describes the total heat production rate in the wave due to HTO, cracking and vaporization.

Similarly, integration of (2.11) across the reaction wave with rates given by (2.14), (2.15) and using the moving coordinate $\xi = x - vt$ yields

$$[m] = v(\gamma_c + \gamma_v). \tag{3.17}$$

Since $[m] = m_v - 1$, we find

$$m_v = 1 + v(\gamma_c + \gamma_v). \tag{3.18}$$

Using (3.13) and (3.14), we write condition (3.8) as

$$\frac{\gamma_h^2(\theta_h + \theta_0)^2 N_h}{Y_{inj}\mathcal{E}_h} \exp\left(-\frac{\mathcal{E}_h}{\theta_h + \theta_0}\right) > 1. \tag{3.19}$$

Together with expression (3.16), all quantities in this condition are expressed through the known problem parameters. The reaction wave parameters are given by (3.14), (3.16) and (3.18). Note that in this solution we did not use any kinetic relations for cracking and vaporization. However, the kinetic coefficients for the HTO reaction are important, as they appear in the necessary condition (3.19). The assumption $v = Y_{inj}/\gamma_h > 1$ yields the inequality (3.1) mentioned above.

3.3 Wave parameters for partial oxygen consumption

Now, let us consider the case when condition (3.8) or, equivalently, (3.19) are not satisfied and, therefore, part of oxygen passes through the HTO layer, such that $Y_{unb} > 0$. This is the only difference relative to the previous case, so the formulae (3.15)–(3.18) are still valid.

Substituting (3.18) into (3.16), we express v as

$$v = \frac{\theta_h - \theta_v}{\theta_h - q - \theta_v(1 - \gamma_c - \gamma_v)}. \tag{3.20}$$

Substituting A_h from (3.7), (3.13) and Z_h from (3.3) into (3.9) we obtain

$$\exp\left(-\frac{\mathcal{E}_h}{\theta_h + \theta_0}\right) = \frac{\mathcal{E}_h v^2}{N_h Y_{inj}(\theta_h + \theta_0)^2}, \tag{3.21}$$

where the speed v is given by (3.20). This is an implicit equation for the HTO temperature θ_h. Because we are considering the reaction-leading structure ($v > 1$) and the condition $Y_{unb} > 0$ in (3.10), we find the wave speed interval $1 < v < Y_{inj}/\gamma_h$. Using (3.16), this range of v determines the interval for θ_h where equation (3.21) must be solved. This can be done numerically. Once θ_h is found, the other wave parameters are determined by (3.10), (3.20).

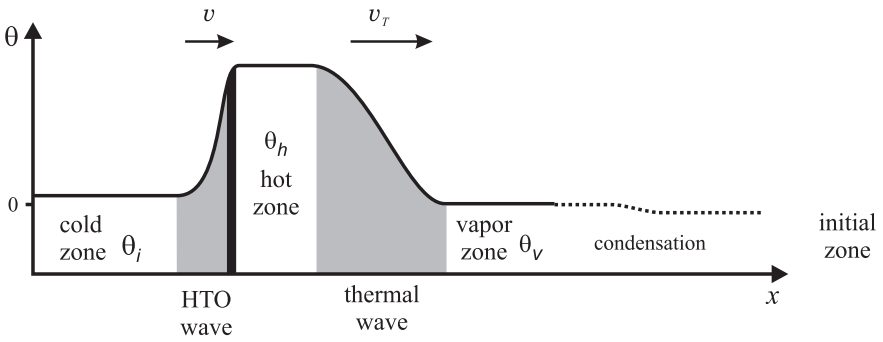

Figure 3: Temperature vs. distance for the reaction-trailing structure. The HTO wave is slower than the thermal wave; a narrow layer where the HTO reaction occurs is shown by the black bar. Cracking and vaporization occur in the thermal wave. The cold zone contains air. The hot zone contains coke and gas with combustion products. The vapor zone contains oleic, aqueous and gaseous phases. The latter contains oil vapor, steam and combustion products.

3.4 Cracking layer

Due to its high activation energy, the cracking reaction in our model occurs in a narrow layer near the corresponding temperature θ_c, see Fig. 2 (narrow dark interval). The analysis of the cracking layer will be presented in short form, because it has much in common with the analysis of the HTO layer. The cracking layer is narrow due to the simple expression taken for cracking rate (2.18). A more realistic study of cracking for distributed medium oil components is presented in A giving a wider cracking layer shown in Fig. 2.

The reaction is mostly confined within a small temperature interval $\delta\theta_c \sim (\theta_h - \theta_v)/Z_c$ with large Zeldovich number $Z_c = \mathcal{E}_c(\theta_h - \theta_v)/(\theta_c + \theta_0)^2 \gg 1$. As in (3.4), the width of the cracking layer is $\delta\xi_c \sim (\theta_h - \theta_v)/Z_c|\theta_c'|$, where $|\theta_c'|$ is the effective temperature gradient in the layer. The analogue of formula (3.9) in this case is

$$v = \frac{(\theta_c + \theta_0)^2 N_c}{2\mathcal{E}_c|\theta_c'|} \exp\left(-\frac{\mathcal{E}_c}{\theta_c + \theta_0}\right). \tag{3.22}$$

The parameters q_c and γ_c describing heat and gas production in cracking are usually very small in applications to in-situ combustion. Then, in the region between the HTO and cracking layers, we can take the approximately constant flux $m = 1$ and drop the heat source term in (3.11), which leads to $(\theta' + (v-1)\theta)' = 0$. Integration in the region between the HTO layer and the cracking layer, where θ, θ' change from θ_c, θ_c' to θ_h, $\theta_{h+}' = -v$ (see Fig. 2), yields the estimate

$$\theta_c' \approx -v + (v-1)(\theta_h - \theta_c). \tag{3.23}$$

The position of the cracking layer in the wave can also be computed, see A.

Using (3.23), equation (3.22) can be solved numerically, furnishing the cracking temperature θ_c. Of course, for the existence of our solution, it is important that the condition $\theta_c < \theta_h$ is satisfied. Otherwise, medium oil remains in the HTO layer and, therefore, participates in the HTO reaction.

4 Reaction-trailing structure

When the coke concentration is large (or oxygen concentration in the injected air is small), so that $Y_{inj} < \gamma_h$ and (3.1) fails, the solution has the structure shown in Fig. 3. The HTO reaction occurs in a slow HTO wave traveling with speed $v < 1$. The temperature in this wave changes from high value θ_h in the hot zone ahead of the wave to the injected air temperature θ_{inj} behind. The cracking reaction and oil vaporization take place in another wave traveling with higher speed v_T. If there were neither medium oil nor light oil/water in the reservoir, this wave would be just a thermal wave with speed $v_T = 1$ similar to that mentioned at the beginning of Section 3. The hot region between the two waves contains coke with dimensionless concentration $n_h = 1$, with neither medium oil nor light oil/water. As in Section 3, we assume that the oil component concentrations n_h^*, n_c^*, n_v^* and the temperature θ_v in the vapor zone ahead of the thermal wave are given.

Since the hot region ahead of the HTO wave contains coke, the oxygen is consumed completely in the HTO reaction. Coke consumption is not necessarily complete, so the HTO reaction is oxygen limited. This solution structure is called reaction-trailing because combustion occurs behind the hot zone.

4.1 HTO wave

High-temperature oxidation is the only reaction in the HTO wave. Such a combustion wave was studied in [15, 24, 31], for instance. Here we present a simpler method for the analysis of this wave, similar to that of Section 3, and we show that there are two different combustion regimes, characterized by complete or partial coke consumption in the HTO reaction. The profile is assumed to have a traveling wave form in the coordinate $\xi = x - vt$. The coke can be partially consumed in the reaction, leaving behind unburned coke with concentration n_h^{unb}. The gas flow is uniform throughout the wave, $m = 1$.

Substitution of w_h from (2.17) into (2.13) with $m = 1$ yields

$$\frac{\partial \log n_h}{\partial t} = -v\,\frac{d\log n_h}{d\xi} = -N_h Y \exp\left(-\frac{\mathcal{E}_h}{\theta+\theta_0}\right). \tag{4.1}$$

The wave contains a narrow HTO layer at about the highest temperature θ_h in the flow. The reaction is confined within a space interval $\delta\xi_h \sim (\theta_h+\theta_0)^2/\mathcal{E}_h|\theta_h'|$, the same as in (3.2), (3.4). Taking $d\log n_h/d\xi_h \sim \log(1/n_h^{unb})/\delta\xi_h$ and $Y \sim Y_{inj}/2$ in (4.1), we obtain

$$v\log(1/n_h^{unb}) \sim A_h \tag{4.2}$$

with the same expression (3.7) for A_h.

The condition for complete coke consumption, $n_h^{unb} \ll 1$, analogous to condition (3.8), takes the form

$$A_h > v. \tag{4.3}$$

In this case the analysis of the HTO wave is completed as in Section 3.2, but the absence of medium and light oil components as well as of water lead to simplification. In the reaction trailing situation we need to replace θ_v by θ_{inj}, m_v by 1, and $q_c = q_v = \gamma_c = \gamma_v = 0$ in the expressions (3.14), (3.13), (3.16), yielding

$$v = \frac{Y_{inj}}{\gamma_h}, \quad |\theta_h'| = \frac{Y_{inj}}{2\gamma_h}, \quad \theta_h = \theta_{inj} + \frac{v}{1-v}. \tag{4.4}$$

Then condition (4.3) takes the form (3.19). Therefore, (3.19) becomes the general condition for complete coke/oxygen consumption in the HTO reaction. Of course, the expression for θ_h to be used in (3.19) in the reaction-leading case (3.16) is different from the reaction-trailing case (4.4).

In the opposite case of incomplete coke consumption, i.e., $A_h < v$, we can take $n_h \sim 1$, i.e., close to the initial concentration, in the HTO layer. Then using $\partial Ym/\partial x = dY/d\xi \sim -Y_{inj}/\delta\xi_h$ with $\delta\xi_h \sim (\theta_h+\theta_0)^2/\mathcal{E}_h|\theta_h'|$ and the reaction rate (2.17) with $n_h \sim 1$ and $Y \sim Y_{inj}/2$ in equation (2.12) yields

$$Y_{inj} = \gamma_h A_h \tag{4.5}$$

with A_h from (3.7). In this equation we took the equality sign disregarding a small error as in (3.9). Integration of (3.11) in the narrow HTO layer as in Section 3.2 yields the temperature gradient $\theta_{h+}' = v(1-n_h^{unb})$ behind the layer and, thus, $|\theta_h'| = v(1-n_h^{unb})/2$. Equation (3.15) takes the form $(v-1)(\theta_h - \theta_{inj}) + v(1-n_h^{unb}) = 0$. Integration of (2.12) with w_h from (2.13) gives $[Y] = -v\gamma_h[n_h]$ or $Y_{inj} = v\gamma_h(1-n_h^{unb})$. As a result, we get

$$n_h^{unb} = 1 - \frac{Y_{inj}}{v\gamma_h}, \quad v = 1 - \frac{Y_{inj}}{\gamma_h(\theta_h - \theta_{inj})}, \tag{4.6}$$

and expression (4.4) for $|\theta_h'|$. Then (4.5) with A_h from (3.7) takes the form

$$\exp\left(-\frac{\mathcal{E}_h}{\theta_h+\theta_0}\right) = \frac{\mathcal{E}_h Y_{inj}}{N_h\gamma_h^2(\theta_h+\theta_0)^2}. \tag{4.7}$$

This equation determines θ_h implicitly and can be solved numerically.

As our analysis leading to (4.2) used only order estimates for the oxygen fraction Y, diffusion has no effect within the accuracy of the method, unless it is dominant in the HTO layer. The latter case may result in extinction and requires a separate study.

4.2 Thermal wave

Cracking and vaporization are heat absorbing processes, which decrease the thermal wave speed: $v_T < 1$. The heat equation (2.10) for a traveling wave depending on the single variable $\xi = x - v_T t$ is (3.11) with $n_h = 0$ and v_T instead of v. Integrating this equation across the wave as in (3.15) taking into account the conditions $[\theta'] = 0$, $[\theta] = \theta_v - \theta_h$, $[m\theta] = m_v\theta_v - \theta_h$, and $[n_c] = [n_v] = 1$, we obtain

$$v_T(\theta_v - \theta_h) - (m_v\theta_v - \theta_h) - v_T(q_c + q_v) = 0. \tag{4.8}$$

The gas flux ahead of the wave is $m_v = 1 + v_T(\gamma_c + \gamma_v)$, as in (3.18). Using this expression in (4.8), we find the wave speed

$$v_T = \frac{\theta_h - \theta_v}{\theta_h - \theta_v(1 - \gamma_c - \gamma_v) + q_c + q_v}. \tag{4.9}$$

Note that the existence of the hot zone between the HTO and thermal waves ensures that complete cracking of the medium oil occurs ahead of the HTO wave.

5 Stability of steady combustion

In this section we study stability of the combustion waves with respect to small perturbations of the dependent variables. The stability problem has a simple solution when oxygen is completely consumed in combustion (both in the complete and partial coke consumption cases). In this case the amount of coke converted is controlled by the injected oxygen flux. Hence, the total conversion rate is not affected by a small perturbation in the temperature profile. This implies that there is no source of instability, and the steady combustion regimes with complete oxygen combustion are stable.

In the case of partial consumption of oxygen, instability may occur leading, for example, to a pulsating combustion regime. Let us consider the case when the cracking and vaporization have a minor effect on the temperature and gas flux, so that the corresponding terms can be neglected in equations (2.10)–(2.13). Then the problem is equivalent to the combustion in a reservoir with a single solid fuel component. Stability analysis for this case with the reaction rate approximated by the Dirac delta function was carried out in [40]. A similar analysis adapted to our model is presented in B.

We assume that a small perturbation of the steady combustion solution depends on time via the complex factor $\exp(\omega t)$. The complex quantity ω is found from the equation derived in B as

$$\begin{aligned}&(v(K-1) + (v-1)\Omega)\sqrt{1+4\Omega}\\ &\quad = v(K - 1 - 2\Omega) + (v-1)(2K-1)\Omega,\end{aligned} \tag{5.1}$$

where

$$\Omega = \frac{\omega}{(v-1)^2}, \quad K = \frac{\mathcal{E}_h(\theta_h - \theta_v)}{(\theta_h + \theta_0)^2}\left(\frac{1}{2} + \frac{\theta_h + \theta_0}{\mathcal{E}_h}\right). \tag{5.2}$$

For $\Omega \neq 0$, equation (5.1) can be reduced to $\Omega^2 + b_1\Omega + b_2 = 0$ with

$$\begin{aligned}b_1 &= -K^2 + K\left(1 + \frac{4v}{v-1}\right) + \frac{(3-4v)v}{(v-1)^2},\\ b_2 &= \frac{v(K-1)(K+v-1)}{(v-1)^2}.\end{aligned} \tag{5.3}$$

The perturbation decays in time when $\operatorname{Re}\omega < 0$, which requires $b_1 > 0$ and $b_2 > 0$. Using Z_h from (3.3) in the second expression in (5.2), we see that $K \sim Z_h/2$. Since $v > 1$ and in the derivations of Section 3 we assumed $Z_h \gg 1$, we conclude that the condition $b_2 > 0$ is satisfied and the condition $b_1 > 0$ yields the stability condition

$$K < \frac{5v - 1 + \sqrt{9v^2 + 2v + 1}}{2(v-1)}. \tag{5.4}$$

This condition implies that the steady combustion regime with partial consumption of oxygen becomes unstable for sufficiently large Zeldovich numbers.

Stability to small perturbations in transverse directions can also be studied. It reduces to the substitution $\Omega \to \Omega + k^2/(v-1)^2$ in (5.1), where k is a wave number of a transverse harmonic perturbation, see [40].

Q_h	3.28×10^7 J/kg
Q_c	3.39×10^5 J/kg
Q_v	1.28×10^6 J/kg,
E_h	1.8×10^5 J/mol (Ref. [41])
K_h	3.05×10^6 1/s (Ref. [41])
E_c	2.5×10^5 J/mol
K_c	4.6×10^{14} 1/s
R	8.314 J/mol K
C_m	2×10^6 J/m^{3}K
λ	0.87 W/mK
c_g	$3.5R$ J/mol K
P_{tot}	10^5 Pa (1 atm)
u_{inj}	1.16×10^{-3} m/s (100 m/day)
M_h	0.012 kg/mol
M_c	0.112 kg/mol
M_v	0.065 kg/mol
$T_{inj} = T_{st}$	293.15 K

Table 1: Typical values of the dimensional parameters for in-situ combustion.

6 In-situ combustion for typical reservoir parameters

Consider the representative reservoir data in Table 1. The numbers quoted there correspond to octene (C_8H_{16}) as a single effective light oil component, to hexadecene ($C_{16}H_{32}$) as a medium oil component, and to an average vaporization heat Q_v for equal mass densities of light oil and water in the vapor zone. We use alkenes for stoichiometric convenience.

Assume that air with an oxygen fraction of $Y_{inj} = 0.21$ is injected into the reservoir. The condition (3.1) written in dimensional form using (2.16) as $n_h^* < Y_{inj} C_m M_h / c_g$ is satisfied for the precoke concentrations $n_h^* < 173$ [kg/m^3] in the vapor zone. This is the case of the reaction-leading wave structure and computations must be carried out using formulae of Section 3. Fig. 4 shows the reaction wave parameters versus the initial precoke concentration n_h^*, when the other parameters in the vapor zone are taken as $n_c^* = 100$ [kg/m^3], $n_v^* = 60$ [kg/m^3], and $T_v = 350$ [K] in $\theta_v = (T_v - T_{st})/T^*$. Complete coke/oxygen consumption in the HTO reaction occurs for high precoke concentrations $n_h^* > 35.5$ [kg/m^3], as found by checking inequality (3.19). For lower precoke concentrations, a considerable part of the injected oxygen passes through the reaction wave, as shown in Fig. 4. The passage from complete to partial oxygen consumption regime is characterized by an abrupt change in the dependence of the variables relative to the coke concentration n_h^*.

Computations show that changes in medium and light oil/water concentrations have a minor influence on the combustion and cracking temperatures θ_h and θ_c. Indeed, the corresponding equations (3.21) and (3.22) have strong exponential dependence on temperature, so the solutions are weakly affected by the change of coefficients. On the contrary, the speed v of the reaction wave decreases when medium and light oil/water concentrations are higher. Extinction occurs when $q = 1 - q_c - q_v$ becomes small, i.e., when the combustion heat $Q_h n_h^*$ becomes close to the heat $Q_c n_c^* + Q_v n_v^*$ necessary for cracking and vaporization. At the extinction point, the speeds of the reaction and thermal waves coincide, i.e., $v \to 1$ in dimensionless form.

Consider now the same reservoir parameters in the vapor zone, but using an injected gas with very low initial oxygen fraction $Y_{inj} = 0.025$. The numerical results are shown in Fig. 5. Condition (3.1) is satisfied for precoke concentrations $n_h^* < 20.6$ [kg/m^3] and corresponds to the case discussed in Section 3. For higher concentrations, the reaction-trailing wave structure occurs and calculations use the formulae of Section 4. These two cases are separated by a resonance point, where the speeds of the two waves coincide: $v = v_T$. The complete coke/oxygen consumption regime is determined by inequality (3.19) and corresponds to a range of initial coke concentrations given by $14.5 < n_h^* < 44.9$ [kg/m^3]. Temperatures in this regime become very high, so that the effects not taken into account in our model may become important, e.g., heat losses. On the contrary, the partial oxygen ($n_h^* < 14.5$ [kg/m^3]) and partial coke ($n_h > 44.9$ [kg/m^3]) consumption regimes are characterized by a more or less constant combustion temperature. When the regime changes, there is a singularity in the dependence of the HTO wave parameters on the initial coke concentration n_h^*.

Fig. 6 presents a chart with different combustion regimes in the (n_h^*, Y_{inj}) plane: coke concentration versus oxygen fraction in injected air. The reaction-leading wave structure is determined by condition (3.1).

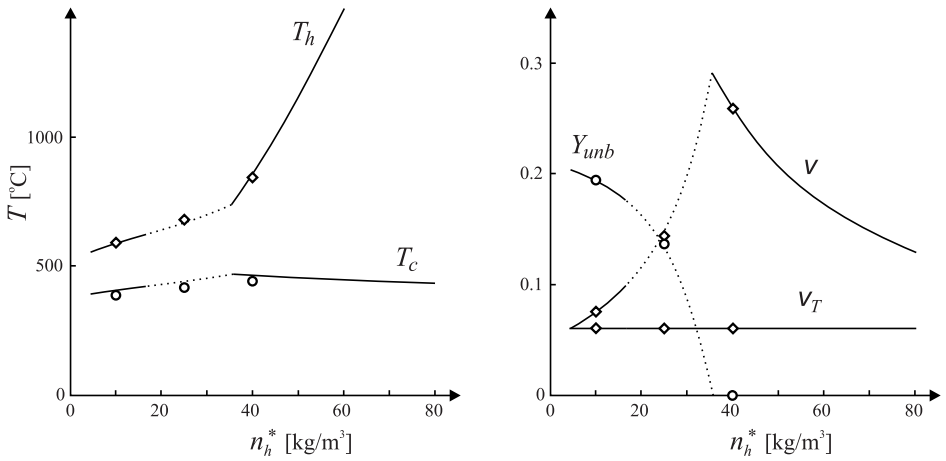

Figure 4: Reaction wave parameters in terms of the coke concentration n_h^* [kg/m^3]. Here we use $n_c^* = 100$ [kg/m^3], $n_v^* = 60$ [kg/m^3] and injection of air with 21% oxygen. The vapor zone temperature is $T_v = 77$ [℃]. Indicated are the hot zone temperature T_h [℃], the cracking temperature T_c [℃], the reaction wave speed v [m/day], the thermal wave speed v_T [m/day], and the unburned oxygen fraction Y_{unb} [mol-O_2/mol-air]. The dotted segments correspond to unstable steady combustion waves. Results of numerical simulations are presented for $n_h^* = 10,\ 25,\ 40$ [kg/m^3] and indicated by diamonds and circles.

In this case condition (3.19) with θ_h from (3.16) determine the combustion regime with complete coke and oxygen consumption. Otherwise, oxygen is only partially consumed. The reaction-trailing wave structure is determined by the opposite of condition (3.1). Then (3.19) with θ_h from (4.4) determines the combustion regime with complete coke and oxygen consumption. Otherwise, coke is partially consumed. Extinction occurs for small n_h^* or small Y_{inj}, when the waves speeds coincide, $v_T = v$. The coincidence of the waves speeds occurs also at the resonance line, see Fig. 6.

Checking numerically the stability condition (5.4), we find oscillatory solutions with partial oxygen consumption in the dark-grey region to the right of the dashed line in Fig. 6. Oscillatory solutions are also indicated by dotted lines in Fig. 4.

The chart of combustion regimes has the qualitative form shown in Fig. 6 for a wide range of parameters. Note that a similar chart of combustion regimes for different parameters (Y_{inj}, m_{inj}) and without instability region was obtained in [15].

6.1 Numerical simulations

We performed direct numerical simulations of the PDE system (2.10)–(2.15) using a split-implicit finite difference numerical scheme. In order to define the vaporization rate w_v, we introduce the molar fraction X of light oil vapor together with steam in the gas. Cracked and vaporized components form the part mX of the total gas flux m. The remaining part $m\,(1-X)$ corresponds to the injected gas flux, which is equal to 1. This gives $X = 1 - 1/m$. As we already mentioned above, the details of the vaporization process have minor influence on the reaction waves of interest here. So we can use a simplified model for numerical purposes that reflects only qualitative properties of vaporization. We take the vaporization rate $w_n = \kappa n_v\,(X_{eq} - X)$ proportional to the liquid oil and water concentration n_v and to the difference between the equilibrium and actual vapor fractions $X_{eq} - X$. The equilibrium vapor fraction is determined by the relation $X_{eq} = \exp\left(h\,(\theta - \theta_b)\right)$, which is the approximation of the Clausius-Clapeyron relation with the linearized exponential expression. The effective boiling temperature θ_b satisfies the equilibrium condition in the vapor zone $X_v = \exp(h(\theta_v - \theta_b))$. The constant coefficients are taken to be $\kappa = 100$, $h = 20$.

The reaction leading and reaction trailing wave structures were observed in numerical simulation for initial temperatures high enough for ignition to occur in a reasonable time span, with different oil concentrations in the initial reservoir and oxygen fractions in the injected gas. The dimensional parameters of the reaction and thermal waves obtained in this simulation are shown in Figs. 4 and 5; we see very good agreement between our approximate solutions and the numerical results.

The combustion waves were found to be stable waves with fixed profile in numerical simulation, except for the case of $n_h^* = 25$ [kg/m^3] in Fig. 4. In the latter case the reaction wave speed v oscillates periodically

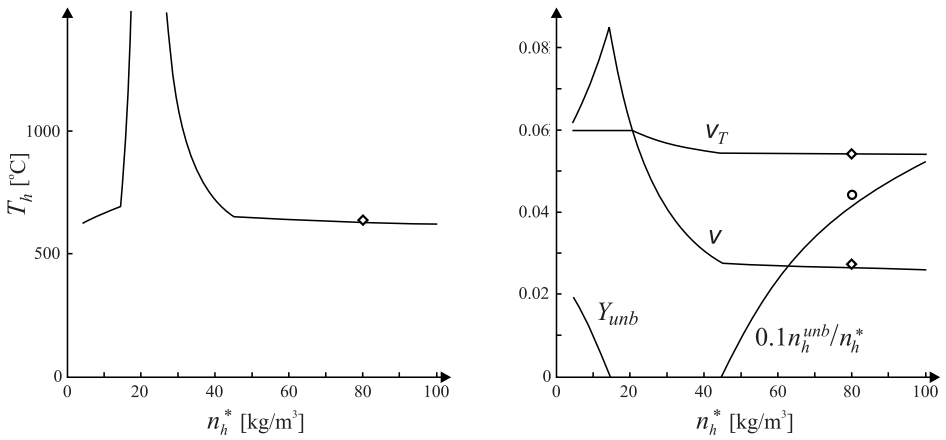

Figure 5: Reaction wave parameters depending on the coke concentration n_h^* [kg/m^3] with $n_c^* = 100$ [kg/m^3], $n_v^* = 60$ [kg/m^3] and injection of air with reduced oxygen (2.5%). Indicated are the hot zone temperature T_h [°C], the HTO and thermal waves speeds v, v_T [m/day], the unburned oxygen fraction Y_{unb}, and the unburned coke fraction n_h^{unb}/n_h^*. The results of numerical simulations are presented for $n_h^* = 80$ [kg/m^3].

in time; Fig. 4 shows the average values of the corresponding quantities. Oscillation amplitudes are about 7% of the average value for T_h and about 30% for v and Y_{unb}. These simulation results agree with the theoretical stability study, see Fig. 6.

7 Conclusions

In this paper, we developed a simplified mathematical approach that provides approximate analytical solutions for steady combustion waves. In this method, rather than explicitly integrating wave equations, we use general estimates and exploit the strong exponential dependence of combustion rate on temperature to simplify the results. This procedure is general and can be applied to the analysis of combustion characterized by large Zeldovich numbers.

This method was used for the analysis of combustion by air injection in porous media containing oil and water, taking into account different chemical and physical processes. The oil is modelled as a composition of three pseudo-components: asphaltenes (precoke), medium and light oil. Precoke is converted to coke at high temperatures, medium oil components are cracked at slightly lower temperatures releasing gaseous oil. Finally, light oil components and water are vaporized. Heat is released in the high-temperature oxidation of coke. Cracking of separate components in the medium oil is also studied (see A).

The solutions are found in the form of sequences of traveling waves. The wave structure is conventionally distinguished according to the position of the hot zone relative to the combustion wave: reaction-leading and reaction-trailing wave structures. The reaction-trailing structure corresponds to high precoke concentrations or low injected oxygen fractions. Otherwise, one finds the reaction-leading structure. Each structure occurs in two different combustion modes. In the first mode, both coke and oxygen are completely consumed in combustion. In the second mode, only a part of oxygen is consumed in the case of the reaction-leading wave structure, or a part of coke is consumed in the case of the reaction-trailing wave structure.

We derived explicit analytical conditions for each combustion regime, stability conditions, and formulae describing dependent variables in the wave sequence solutions. Additionally we described the internal structure of the oil cracking layer for the reaction-leading wave structure.

Numerical computations with typical reservoir data for in-situ combustion lead to the following observations. The most typical wave structure is reaction-leading. With increasing coke concentration, a mode with partial oxygen consumption changes into a mode with complete coke/oxygen consumption. The first mode is characterized by a weak dependence of the combustion temperature on the reservoir parameters, while temperatures may become much higher in the mode with complete coke/oxygen consumption. The reaction-trailing structure can also be found when the injected air contains reduced oxygen fractions (for example, for injection of a mixture of air and flue gases). It is shown that instability can only occur in the regime with partial oxygen consumption. Numerical simulation of the full system of governing equations was carried out showing the expected accuracy of our asymptotic formulae; the simulations confirmed the

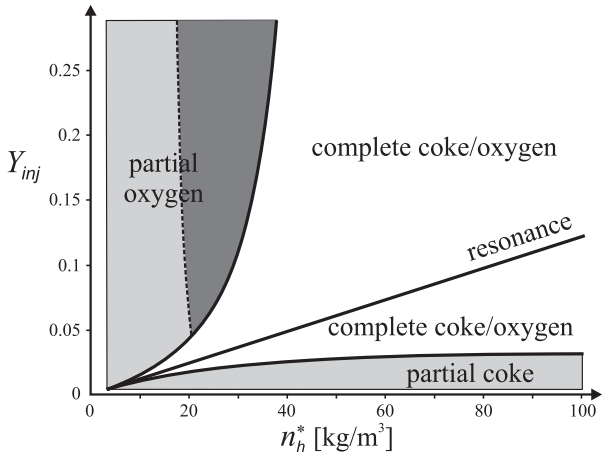

Figure 6: Chart of coke and oxygen consumption in combustion regimes for different coke concentrations n_h^* [kg/m^3] and injected oxygen fractions Y_{inj}. Resonant states form a straight line that separates combustion regimes with different wave structures: reaction-leading (above the line) and reaction-trailing (below the line). The grey regions correspond to combustion regimes with partial oxygen or partial coke consumption. The upper dark grey region to the right of the dashed line corresponds to oscillatory solutions. The white region corresponds to essentially complete coke and oxygen consumption. Thin white strips near the axes correspond to extinction.

existence of combustion in a periodically pulsating wave in the instability region.

A Cracking of multiple components

More realistic description of cracking process requires considering a distribution of hydrocarbon components in the medium oil. Let us denote these components by the index α with corresponding dimensionless concentrations $n_{c\alpha}$ normalized so that $n_{c\alpha} = 1$ downstream in the vapor zone. The cracking rate $w_{c\alpha}$ of each component is described by expression (2.18) with specific kinetic coefficients $N_{c\alpha}$ and $\mathcal{E}_{c\alpha}$. Finally, one should write (2.14) in the form $\partial n_{c\alpha}/\partial t = -w_{c\alpha}$ and substitute $q_c w_c$ by $\sum_\alpha q_{c\alpha} w_{c\alpha}$ and $\gamma_c w_c$ by $\sum_\alpha \gamma_{c\alpha} w_{c\alpha}$ in (2.10), (2.11).

Each medium oil component cracks independently near the corresponding temperature $\theta_{c\alpha}$ within the cracking layer, see Fig. 2. An analysis similar to that in Section 3.4 yields an equation similar to (3.22):

$$v = \frac{(\theta_{c\alpha} + \theta_0)^2 N_{c\alpha}}{2\mathcal{E}_{c\alpha}|\theta'_{c\alpha}|} \exp\left(-\frac{\mathcal{E}_{c\alpha}}{\theta_{c\alpha} + \theta_0}\right). \tag{A.1}$$

The temperature gradient $\theta'_{c\alpha}$ must be estimated by solving the heat balance equation ahead of the HTO layer. The approximate form of this equation is $(\theta' + (v-1)\theta)' = 0$, as shown in Section 3.4. Integration yields the relation

$$\theta'_{c\alpha} = -v + (v-1)(\theta_h - \theta_{c\alpha}) \tag{A.2}$$

similar to (3.23). Using (A.2), equation (A.1) can be solved numerically for $\theta_{c\alpha}$ giving the cracking temperature of component α. Setting $\xi = 0$ in front of the HTO layer, where $\theta(0) = \theta_h$ and $\theta'(0) = \theta'_{h+} = -v$, we find

$$\theta(\xi) = \theta_h + \frac{v - v\exp((1-v)\xi)}{1-v}. \tag{A.3}$$

Given $\theta(\xi_\alpha) = \theta_{c\alpha}$, this equation determines the position ξ_α of the α-component cracking layer in the wave.

B Stability analysis

The analysis below applies the method developed in [40] to the model under consideration. We study the reaction-leading wave structure when all coke and part of oxygen burn in the HTO layer ($v > 1$). When cracking and vaporization are neglected ($w_c = w_v = 0$), equation (2.11) yields $\partial m/\partial x = 0$, so the gas flux is

fixed by the injection condition and by our choice of nondimensional parameters as $m = 1$. The temperature profile is governed by equation (2.10) taking the form

$$\frac{\partial\theta}{\partial t} + \frac{\partial\theta}{\partial x} = \frac{\partial^2\theta}{\partial x^2} + w_h. \tag{B.1}$$

The HTO layer is narrow. Neglecting its width, we can write the reaction rate as proportional to Dirac's delta function $\delta(x)$. Using (2.13) with n_h changing from the initial value 1 to 0 (complete consumption of coke), we find

$$w_h(x,t) \approx \delta(t - t_h(x)) = \frac{dx_h}{dt}\,\delta(x - x_h(t)), \tag{B.2}$$

where $x = x_h(t)$ denotes the HTO layer position at time t, and $t = t_h(x)$ is its inverse. The second equality in (B.2) exploits transformation properties of delta functions. Note that the assumption of a single narrow HTO layer is valid for small perturbations considered in our stability analysis. However, as indicated in [35], there is no clear relationship between the value of $\delta\xi_h$ in (3.4) and the width of the HTO layer for pulsating fronts.

The delta function (B.2) in (B.1) is balanced by the second derivative. This implies a jump of the first derivative of the temperature at the HTO layer and the continuity of the temperature θ. That is,

$$\theta_+ = \theta_-, \quad \left(\frac{\partial\theta}{\partial x}\right)_+ - \left(\frac{\partial\theta}{\partial x}\right)_- = -\frac{dx_h}{dt}, \tag{B.3}$$

where the subscripts $\pm$ denote the values on different sides of the HTO layer, $x \to x_h(t) \pm 0$. The third condition is (3.9) with A_h from (3.7), $v = dx_h/dt$, and $\theta_h = \theta_+ = \theta_-$:

$$\frac{dx_h}{dt} = \frac{(\theta_- + \theta_0)^2 N_h Y_{inj}}{2\mathcal{E}_h|\theta_h'|}\exp\left(-\frac{\mathcal{E}_h}{\theta_- + \theta_0}\right). \tag{B.4}$$

Expressing dx_h/dt from (B.3) and taking $2\theta_h' \sim (\partial\theta/\partial x)_- + (\partial\theta/\partial x)_+$, which is negative, we write this condition as

$$\left(\frac{\partial\theta}{\partial x}\right)_+^2 - \left(\frac{\partial\theta}{\partial x}\right)_-^2 = \frac{(\theta_- + \theta_0)^2 N_h Y_{inj}}{\mathcal{E}_h}\exp\left(-\frac{\mathcal{E}_h}{\theta_- + \theta_0}\right). \tag{B.5}$$

The steady solution $\theta(x,t) = \theta_0(\xi)$ with $\xi = x - vt$ was found in Section 3.3. With the simplifications stated above, the steady solution is determined by equations (B.1)–(B.3) as

$$\begin{aligned} &\theta_0(\xi) = \theta_v + (\theta_h - \theta_v)\exp(-(v-1)\xi) \quad \text{for } \xi > 0; \\ &\theta_0(\xi) = \theta_h \quad \text{for } \xi < 0. \end{aligned} \tag{B.6}$$

The temperature θ_h is found from (B.3), (B.6) as

$$\theta_h - \theta_v = v/(v-1) \tag{B.7}$$

in agreement with (3.20) for $q = 1$ from (3.16). The speed v is determined by (3.21), which can also be derived from (B.5)–(B.7).

Consider small perturbation of the temperature profile and the HTO layer position in the form

$$\theta(x,t) = \theta_0(\xi) + \theta_1(\xi)\exp(\omega t), \quad x_h(t) = vt + \varepsilon\exp(\omega t). \tag{B.8}$$

The latter also implies the change of inequalities in (B.6) as $\xi > \varepsilon\exp(\omega t)$ and $\xi < \varepsilon\exp(\omega t)$. We are looking for solutions with $\operatorname{Re}\omega > 0$. Such solutions grow in time and imply the instability of the steady combustion wave. Equation (B.1) with $w_h = 0$ for $x \neq x_h$ gives the bounded solution as

$$\begin{aligned} &\theta_1(\xi) = A\exp(z_1\xi) \quad \text{for } x > x_h(t); \\ &\theta_1(\xi) = B\exp(z_2\xi) \quad \text{for } x < x_h(t), \end{aligned} \tag{B.9}$$

with

$$z_1 = -\frac{v-1}{2}(1 + \sqrt{1+4\Omega}), \quad z_2 = -\frac{v-1}{2}(1 - \sqrt{1+4\Omega}) \tag{B.10}$$

and Ω defined in (5.2).

For $x > x_h$, using (B.8) and the first expressions in (B.6), (B.9), we obtain

$$\begin{aligned} \theta(x,t) &= \theta_v + (\theta_h - \theta_v)\exp(-(v-1)(x-vt)) \\ &\quad + A\exp(z_1(x-vt)+\omega t). \end{aligned} \tag{B.11}$$

Assuming that A, B and $x_h - vt = \varepsilon\exp(\omega t)$ are small, and considering the limit $x \to x_h(t) + 0$, we find up to first order terms

$$\begin{aligned} \theta_+ &= \theta_h - (\theta_h - \theta_v)(v-1)\varepsilon\exp(\omega t) + A\exp(\omega t) \\ &= \theta_h + (A - v\varepsilon)\exp(\omega t), \end{aligned} \tag{B.12}$$

where the last equality follows from (B.7). Analogous derivations using the second expressions in (B.6), (B.9) in the limit $x \to x_h(t) - 0$ yield

$$\theta_- = \theta_h + B\exp(\omega t). \tag{B.13}$$

For spacial derivatives, the corresponding limits are found similarly as

$$\begin{aligned} \left(\frac{\partial\theta}{\partial x}\right)_+ &= -v + \left(z_1 A + \frac{v^2\varepsilon}{\theta_h - \theta_v}\right)\exp(\omega t), \\ \left(\frac{\partial\theta}{\partial x}\right)_- &= z_2 B\exp(\omega t). \end{aligned} \tag{B.14}$$

Substituting (B.12)–(B.14) and x_h from (B.8) into (B.3), (B.5), zero order terms cancel due to (3.21), and for first order terms we obtain equations

$$A - v\varepsilon = B, \tag{B.15}$$

$$z_1 A + v^2\varepsilon/(\theta_h - \theta_v) - z_2 B = -\omega\varepsilon, \tag{B.16}$$

$$\begin{aligned} -2v(z_1 A + v^2\varepsilon/(\theta_h - \theta_v)) = \\ = N_h Y_{inj}\exp\left(\frac{-\mathcal{E}_h}{\theta_h + \theta_0}\right)\left(1 + \frac{2(\theta_h + \theta_0)}{\mathcal{E}_h}\right)B. \end{aligned} \tag{B.17}$$

Multiplying both sides of (B.17) by $(\theta_h - \theta_v)/2v^2$ and using (3.21), we find

$$-(\theta_h - \theta_v)z_1 A/v - v\varepsilon = KB \tag{B.18}$$

with K defined in (5.2). Equations (B.15), (B.16), (B.18) have nonzero solution for A, B, ε if the determinant of the coefficient matrix vanishes. Using (B.7) and (B.10), this gives equation (5.1).

References

[1] J. H. Abou-Kassem, S. M. Farouq Ali, J. Ferrer, Appraisal of steamflood models, Rev. Tec. Ing., Univ. Zulia 9 (1986) 45–58.

[2] S. Akin, M. V. Kok, S. Bagci, O. Karacan, Oxidation of heavy oil and their SARA fractions: Its role in modeling in-situ combustion, Society of Petroleum Engineers Paper 63230.

[3] L. M. Castanier, W. E. Brigham, Modifying in-situ combustion with metallic additives, In Situ 21 (1) (1997) 27–45.

[4] L. M. Castanier, W. E. Brigham, Upgrading of crude oil via in situ combustion, Journal of Petroleum Science and Engineering 39 (2003) 125–136.

[5] M. V. Kok, C. O. Karacan, Behavior and effect of SARA fractions of oil during combustion, SPE Reservoir Evaluation and Engineering 3 (2000) 380–385.

[6] C. Y. Lin, W. H. Chen, W. E. Culham, New kinetic models for thermal cracking of crude oils in in-situ combustion processes, SPE Reservoir Engineering 2 (1987) 54–66.

[7] C. Y. Lin, W. H. Chen, S. T. Lee, W. E. Culham, Numerical simulation of combustion tube experiments and the associated kinetics of in-situ combustion processes, SPE Journal 24 (1984) 657–666.

[8] S. Whitaker, Simultaneous heat, mass and momentum transfer in porous media: a theory of drying, Advances in Heat Transfer 13 (1) (1977) 19–203.

[9] Y. B. Zeldovich, G. I. Barenblatt, V. B. Librovich, G. M. Makhviladze, The mathematical theory of combustion and explosion, Consultants Bureau, New York, 1985.

[10] A. A. M. Oliveira, M. Kaviany, Nonequilibrium in the transport of heat and reactants in combustion in porous media, Progress in Energy and Combustion Science 27 (5) (2001) 523–545.

[11] M. G. Gerritsen, L. J. Durlofsky, Modeling fluid flow in oil reservoirs, Annual Review of Fluid Mechanics 37 (2005) 211–238.

[12] M. R. Kristensen, M. G. Gerritsen, P. G. Thomsen, M. L. Michelsen, E. H. Stenby, Efficient integration of stiff kinetics with phase change detection for reactive reservoir processes, Transport in Porous Media 69 (2007) 383–409.

[13] P. C. Bowes, P. H. Thomas, Ignition and extinction phenomena accompanying oxygen-dependent self-heating of porous bodies, Combustion and Flame 10 (1966) 221–230.

[14] A. A. Mailybaev, J. Bruining, D. Marchesin, Analytical formulae for in-situ combustion, Proceedings – 17th SPE Symposium on Improved Oil Recovery Symposium 2 (2010) 1120–1135, SPE 129904 (to appear in SPE Journal).

[15] D. A. Schult, B. J. Matkowsky, V. A. Volpert, A. C. Fernandez-Pello, Forced forward smolder combustion, Combustion and Flame 104 (1996) 1–26.

[16] D. A. Schult, A. Bayliss, B. J. Matkowsky, Traveling waves in natural counterflow filtration combustion and their stability, SIAM J. Appl. Math. 58 (1998) 806–852.

[17] A. P. Aldushin, B. J. Matkowsky, D. A. Schult, Downward buoyant filtration combustion, Combustion and Flame 107 (1996) 151–175.

[18] A. P. Aldushin, B. J. Matkowsky, D. A. Schult, Buoyancy driven filtration combustion, Combustion Science and Technology 125 (1997) 283–349.

[19] A. P. Aldushin, A. Bayliss, B. J. Matkowsky, On the transition from smoldering to flaming, Combustion and Flame 145 (2006) 579–606.

[20] A. P. Aldushin, I. E. Rumanov, B. J. Matkowsky, Maximal energy accumulation in a superadiabatic filtration combustion wave, Combustion and Flame 118 (1999) 76–90.

[21] A. Bayliss, B. J. Matkowsky, From traveling waves to chaos in combustion, SIAM J. Appl. Math. 54 (1994) 147–174.

[22] B. J. Matkowsky, G. Sivashinsky, Propagation of a pulsating reaction front in solid fuel combustion, SIAM J. Appl. Math. 35 (1978) 465–478.

[23] I. Y. Akkutlu, Y. C. Yortsos, The dynamics of in-situ combustion fronts in porous media, Combustion and Flame 134 (2003) 229–247.

[24] C. W. Wahle, B. J. Matkowsky, A. P. Aldushin, Effects of gas-solid nonequilibrium in filtration combustion, Combust. Sci. and Tech. 175 (2003) 1389–1499.

[25] M. Fatehi, M. Kaviany, Adiabatic reverse combustion in a packed bed, Combustion and Flame 99 (1) (1994) 1–17.

[26] D. Shin, S. Choi, The combustion of simulated waste particles in a fixed bed, Combustion and flame 121 (1–2) (2000) 167–180.

[27] G. D. Adaguin, I. Y. Akkutlu, Influence of in situ fuel deposition on air injection and combustion processes, Journal of Canadian Petroleum Technology 46 (4) (2007) 54–61.

[28] M. F. Martins, S. Salvador, J. F. Thovert, G. Debenest, Co-current combustion of oil shale – Part 1: Characterization of the solid and gaseous products, Fuel 89 (1) (2010) 144–151.

[29] M. F. Martins, S. Salvador, J. F. Thovert, G. Debenest, Co-current combustion of oil shale – Part 2: Structure of the combustion front, Fuel 89 (1) (2010) 133–143.

[30] H. Byrne, J. Norbury, The effect of solid conversion on travelling combustion waves in porous media, Journal of Engineering Mathematics 32 (1997) 321–342.

[31] J. Bruining, A. A. Mailybaev, D. Marchesin, Filtration combustion in wet porous medium, SIAM J. Appl. Math. 70 (2009) 1157–1177.

[32] D. N. Dietz, J. Weijdema, Wet and partially quenched combustion, Journal of Petroleum Technology 20 (1968) 411–415.

[33] J. Weijdema, Zur oxydationskinetik kohlenwasserstoffe in porösen medien in bezug auf untererdische verbrennung, Erdöl und Kohle, Erdgas Petrochemie 21 (1968) 520–526.

[34] D. A. Schult, V. A. Volpert, Linear stability analysis of thermal free radical polymerization waves, International Journal Of Self Propagating High Temperature Synthesis 8 (4) (1999) 417–440.

[35] S. A. Cardarelli, D. Golovaty, L. K. Gross, V. T. Gyrya, J. Zhu, A numerical study of one-step models of polymerization: Frontal versus bulk mode, Physica D: Nonlinear Phenomena 206 (3–4) (2005) 145–165.

[36] J. L. Torero, Buoyancy Effects on Smoldering of Polyurethane Foam, Ph.D. thesis, Dept. Mech. Eng., University of California, Berkeley, CA, 1992.

[37] A. P. Aldushin, Heat transfer and convection combustion regimes of porous systems with filtration of heat carrier, Combustion, Explosion, and Shock Waves 26 (2) (1990) 180–187.

[38] D. A. Schult, B. J. Matkowsky, V. A. Volpert, A. C. Fernandez-Pello, Propagation and extinction of forced opposed flow smolder waves, Combustion and Flame 101 (4) (1995) 471–490.

[39] G. Debenest, V. V. Mourzenko, J. F. Thovert, Smouldering in fixed beds of oil shale grains: governing parameters and global regimes, Combustion Theory and Modelling 9 (2) (2005) 301–321.

[40] A. P. Aldushin, S. G. Kasparyan, Stability of stationary filtrational combustion waves, Combustion, Explosion, and Shock Waves 17 (6) (1981) 615–625.

[41] I. W. Smith, The intrinsic reactivity of carbons to oxygen, Fuel 57 (1978) 409–414.